Roughness Analysis of Local Fatigue Fracture Surface

Stepan Major and Stepan Hubalovsky

***Abstract*—** A stereophotogrammetrical analysis in scan electron microscopy is used to investigate the fracture morphology of the high-strength low-alloy steel generated under combined bending-torsion fatigue loading. The type of loading is described by loading ratio $Z= \tau_a / (\sigma_a + \tau_a)$ (σ_a is the bending amplitude and τ_a is the torsion amplitude). The fatigue life of investigated specimens was in the order of 10^6 cycles (high cycle fatigue). Roughness characteristics studied in two mutually perpendicular directions on facets in the region of crack initiation were found to be sensitive to the crack front positron. The investigation of surface topography revealed the presence of the opening Mode *I* in all investigated crack front locations.

***Keywords*—** Bending-Torsion, Fractography, Biaxial loading, Fatigue, Fracture Surface

I. Introduction

THIS article deals with quantitative analysis of fracture surface generated by fatigue. A schematic fracture surface map is a valuable result of visual or microscopic observation. It seeks to isolate and identify the features on the surface which show how the sample failed. Such a map can be a valuable way of presenting information which shows clearly how a crack was initiated and how grew with time. Currently scanning electron microscopy showed numerous microcracks and other details of fracture surface topology. Images obtained by scanning electron microscopy can be used for the three-dimensional reconstruction of object [1]. Quantitative fractography has been used as a tool in material research from seventieth last century. The fracture surface can be considered to be a degradation process the gauge [1-7]. Quantitative fractography has been shown to be outstanding importance for understanding ductile and cleavage fracture, determining fracture mechanism in metallic materials, acquiring information of details needed for making progress in fracture mechanics [1-3]. For example first applications on steel [1] showed that fracture surfaces originating at varying conditions differ significantly in their quantitative characteristics. Two-dimensional characteristics were mostly used via stereo-photogrammetry [4-5].

The fracture surface roughness depends on loading Mode. Tension loads produce Mode I or opening loads. This is most common loading. Torsion loading of a surface crack produces both Mode II and Mode III. The surface roughness usually extremely enhanced when a high portion of lower to medium amplitudes of shear loading modes II and III is applied [1-2,6-8]. In such cases the crack usually propagates in extremely complicated manner making local arrests and forming branch/twist morphology or so-called factory roofs [6-8]. For this surface are typical such geometrical formation as steps and facets. In the contrary a high amount of opening loading mode or, sometimes, a high-amplitude of shear loading lead to a macroscopically flat surface.

The efforts to approach fractography in a more quantitative way has led to many interesting studies on the interconnection between the surface morphology and loading conditions. However, the most crucial problem in the quantitative fractography remains to be a significant lack of experimental data from fracture surfaces created by multiaxial loading [9,10]. Roughness parameters (for example R_V , R_a or R_L) significantly increased above a critical value of loading ratio $Z_c \approx 0.5$ (the torsion loading component is equal to the bending one). The roughness parameters were calculated for long profiles (length 0.4mm). This long profiles covered lot of steps and facets. Therefore, their roughness parameters are not able to described properties of individual geometrical formation as steps and facets. This paper deals with details of the morphology produced by a combined bending-torsion loading and investigation of surface topography revealed the presence of the opening Mode I in all investigated crack front locations.

II. Experimental procedure

The sinusoidal bending-torsion loading ($R= -1$) was applied to smooth cylindrical specimens made of the high-strength low-alloy Cr-Al-Mo steel. Its mechanical properties of are $\sigma_u = 950$MPa. Loading settings and achieved fatigue life data are collected in Table 1. The fatigue tests were made using the fatigue machine MZGS -100 of the polish origin at the room temperature. Fig. 1 shows geometry of specimen.

Stepan Major is working at the Institute of Theoretical and Applied Mechanics, Academy of Science, 190 00 Praha, Prosecka 809/76, Czech Republic, s.major@seznam.cz.

Stepan Hubalovsky is working at University of Hradec Kralove, Department of informatics, Faculty of Science, Hradec Kralove 500 38, Rokitanskeho 62, Czech republic, stepan.hubalovsky@uhk.cz.

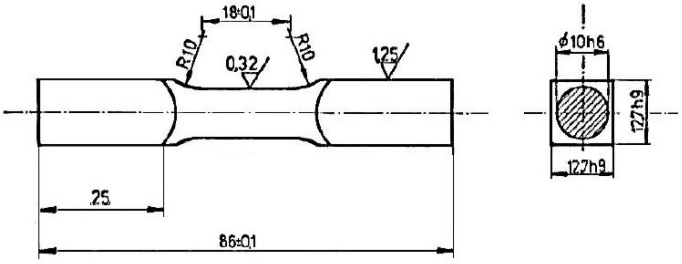

Fig.1. Geometry of the specimen

Table 1 Experimental data – loading history : τ_a amplitude of shea loading, τ_a bending amplitude if of shea loading., *Nf* number of coefficient of loading, coincidence of loading $Z = \tau_a /(\tau_a + \sigma_a)$ cycle to failure [11,12,13] (Bending-torsion : B-T, Pure torsion: PT, Pure bending: PB):

Loading	σ_a [MPa]	τ_a [MPa]	Z [−]	N_f [10^3]
PB	620	0	0	4475
B-T	396	132	0.25	1478
B-T	245	246	0.5	1635
B-T	140	385	0.73	1229
PT	0	390	1	1715

III. Stereophotogrametry and Three-dimensional Reconstruction of Fracture Surface

The analyzed areas are at a distance about 1 mm from the crack initiation on the specimen surface. Three-dimensional data of the surface morphology were obtained by means of the stereo-photogrammetry [3-4] using the scanning electron microscope Leo S440 and the commercial software Alicona MeX (Alicona. GmbH, Graz, Austria). The measurements were made in the Erich Schmid Institute of Materials Science (Leoben, Austria). Stereoimages were taken with magnification 200 for global roughness analysis and 800 for local study of facets and steps. Stereoimages were taken by tilting the specimen by an angle 7º-10º in dependence on local surface relief complexity. The output of elevation models consisted of up to 500000 nonequidistantly localized points. For global analysis the square area of size 0.16 mm2 was chosen with its centre at the distance of 0.8 mm from the crack initiation. Using Delauny triangulation [11], two sets of 50 profiles were traced for all analyzed areas. In order to evaluate different position of the progressing macrocrack front, the first set laid in the crack propagation direction and the second one perpendicular to this direction. Selected profiles for local analysis are shown on Fig.2. The morphology of pure bending specimen and for first two bending-torsion specimen is geometry very similar (For this reason we show only the first of the fracture surface of the sample. geometric formulation of profiles in all three cases, virtually the same.).

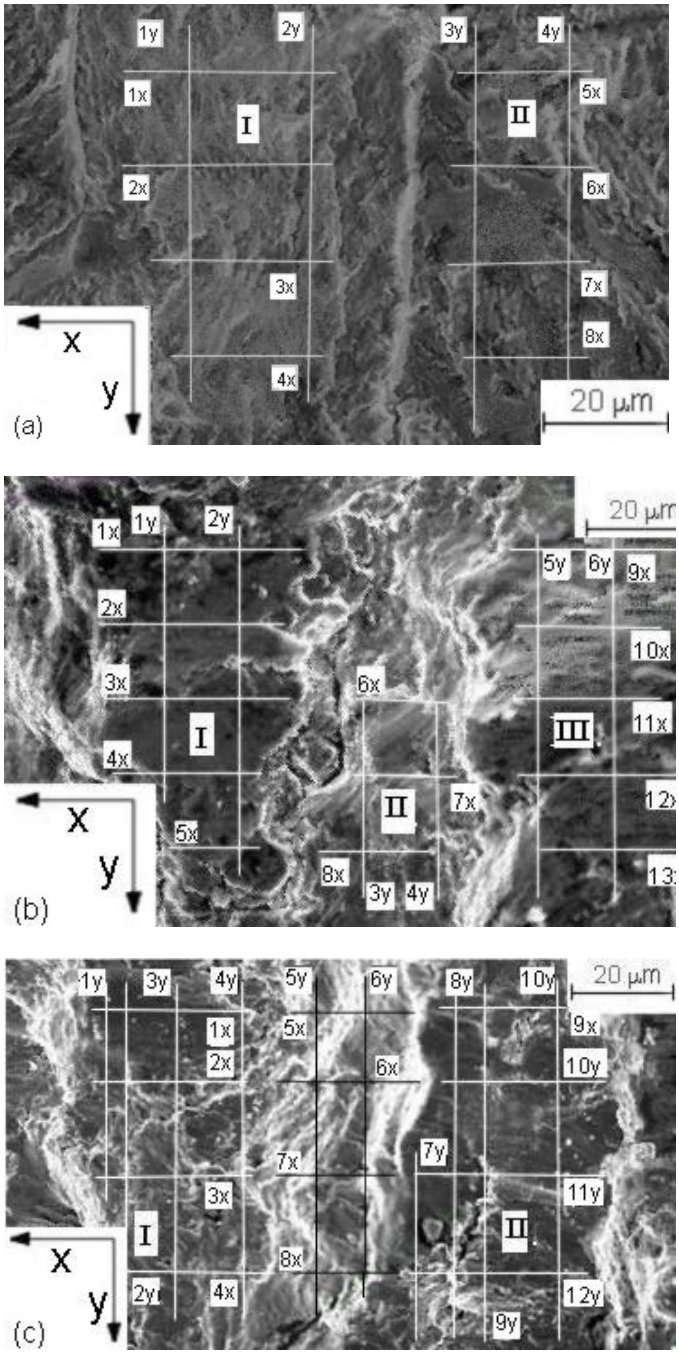

Fig.2 Details of fatigue fracture surface. The crack initiation site on the specimen surface is at distance at about 1mm in the negative X-direction. Type of loading: (a) PB, pure-bending, Z_c = 0; (b) B-T, combined torsion-bending, Z_c = 0.73, (c) PT, pure-torsion Z_c = 1.

IV. Fractography and Roughness Parameters

A. Roughness parameters

In order to evaluate different aspect of roughness, several types of parameters were adapted. Probably most frequently used roughness parameter is maximum valley depth R_V, which is defined as ratio of sum of height differences between adjacent profile points to projected profile length [12, 13]:

$$R_V = \frac{1}{L_P}\sum_{i=1}^{N-1}\left(y_{i+1} - y_i\right) \quad (1)$$

Where L_P is projected profile length and y_i is height of adjacent profile points.

One often used example of amplitude parameter is average height R_a of primary profile [12, 12, 13]:

$$R_a = \frac{1}{N}\sum_{i=1}^{N}\left|y_i - y_m\right|. \quad (2)$$

where N is a number of points, y_i and y_m are vertical surface coordinates and their mean value. Another roughness parameters are based on central moments of the probability density function $p(z)$ of surface heights. The average height is one of amplitude parameters. Profile amplitude parameters depending only on changes in vertical z-coordinate are represented by the arithmetic roughness R_a and the vertical profile range R_z, which is simply given as a difference between the highest and the lowest points of the profile. The central moment of k-order can be written as [12, 12, 13]:

$$\mu_k = \frac{1}{N}\sum_{i=1}^{N}\left(y_i - y_m\right)^k . \quad (3)$$

Representatives of second, third and fourth central moments are root mean square roughness R_q, skewness R_{Sk} and kurtosis R_{ku} of primary profile [10,12, 12, 13]:

$$R_q = \sqrt{\mu_2}$$
$$R_{Sk} = \frac{\mu_3}{\mu_2^{3/2}} \quad (4)$$
$$R_{Ku} = \frac{\mu_4}{\mu_2^2} - 3$$

B. Fractal parameters

A fractal dimension is an index for characterizing fractal patterns by quantifying their complexity of system as a ratio of the change in detail to the change in scale. Several types of fractal dimension can be measured theoretically and empirically. Fractal dimensions are used to characterize a broad spectrum of objects ranging from the abstract to practical phenomena to quantitative fractography.

For the description of fractal properties of surface or profile are often used fractal dimension. The concept of a fractal dimension rests in unconventional views of scaling and dimension. Such familiar scaling relationships can be defined mathematically as:

$$N \propto \varepsilon^N \quad (5)$$

where the variable N stands for the number of new sticks, ε for the scaling factor, and D for the fractal dimension.

Other fractal characteristic often used in fractography is Hurst exponent. The generalized Hurst exponent, has been denoted by H in honor of both Harold Edwin Hurst (1880–1978). H is directly related to fractal dimension, D, and is a measure of a data series' "mild" or "wild" randomness.

V. Analysis of Fracture Surface

Profiles in two mutually perpendicular directions were compiled in order to cover uniformly both investigated facets as it is shown in Fig.3a (pure-bending). In this case in comparison to torsion loading and torsion-bending loading are facet not clear. Along the *Y*-direction, the facet I twists from the macroscopic (horizontal) plane by an angle of 7° - see Fig. 3a (pure-bending). Twist angle of facet II is the same as that of the facet I. Calculated values of roughness parameters are summarized in Table 2.

The roughness values R_V, R_{Sk} and R_{ku} in the direction of the crack growth (profiles x1, x2, x3 and x4) are, in average, distinctly higher than those in the direction of the crack front (profiles 1y to 8y). The fracture surface caused pure bending loading size up to be macroscopically very flat, however the roughness parameters calculated for facets closed case of pure torsion and combined loading in the case that $Z_C \leq 0.6$ [11].

In the case bending-torsion Z = 0.25, Along the Y-direction, the facet I twists from the macroscopic (horizontal) plane by an angle of 10°, Twist angle of facet II is -1°. Calculated values of roughness parameters are summarized in Table 2.

In the case bending-torsion Z = 0.25, Along the Y-direction, the facet I twists from the macroscopic (horizontal) plane by an angle of 10°, Twist angle of facet II is -1°. Calculated values of roughness parameters are summarized in Table 3.

In the case bending-torsion Z_C = 0.5, Along the Y-direction, the facet I twists from the macroscopic (horizontal) plane by an angle of −8°, Twist angle of facet II is 5°. Calculated values of roughness parameters are summarized in Table 4.

In all this cases of fractal characteristic no dependence between loading and D or H was observed.

Table 2. Profile roughness - pure bending.

Pr	R_V	R_a [μm]	R_q [μm]	R_{Sk}	R_{ku}	H	D
1y	0.69	4.56	4.24	−0.35	−0.85	0.8	1.03
2y	0.79	6.10	6.41	−0.75	−0.93	0.7	1.02
3y	0.53	3.45	5.49	1.22	1.63	0.7	1.02
4y	0.66	3.58	3.86	0.55	−1.34	0.7	1.04
1x	0.64	2.53	3.35	0.87	−1.30	0.7	1.03
2x	0.64	2.59	3.92	−0.04	−1.34	0.8	1.02
3x	0.36	3.21	4.32	1.18	1.20	0.7	1.02
4x	0.48	2.85	3.21	0.60	−1.45	0.7	1.00
5x	0.73	4.20	4.73	−0.07	−0.51	0.7	1.00
6x	0.43	2.27	2.90	0.48	−1.30	0.8	1.03
7x	0.49	1.11	1.58	0.50	−0.83	0.7	1.04
8x	0.46	3.83	4.11	0.80	−1.43	0.6	1.01

Table 3. Profile roughness − bending−torsion $Z = 0.25$.

Pr	R_V	R_a [μm]	R_q [μm]	R_{Sk}	R_{ku}	H	D
1y	0.65	3.68	5.27	−0.47	−0.89	0.9	1.01
2y	0.68	7.18	5.42	−0.86	−0.87	0.6	1.09
3y	0.69	3.24	4.98	1.85	1.72	0.6	1.02
4y	0.48	2.82	4.02	0.48	−1.31	0.8	1.15
1x	0.54	2.25	3.01	0.76	−1.48	0.8	1.03
2x	0.36	1.98	2.42	−0.0	−1.42	0.8	1.27
3x	0.38	2.02	3.32	0.98	−0.98	0.2	1.09
4x	0.32	1.86	3.25	0.42	−1.05	0.63	1.05
5x	0.42	3.52	3.92	−0.03	−0.91	0.9	1.08
6x	0.38	2.03	3.95	0.38	−1.36	0.8	1.07
7x	0.52	2.15	1.48	0.65	−0.76	0.65	1.02
8x	0.87	1.42	6.15	0.89	2.01	0.7	1.12

Table 4. Profile roughness − bending−torsion $Z = 0.5$.

Pr	R_V	R_a [μm]	R_q [μm]	R_{Sk}	R_{ku}	H	D
1y	0.38	4.32	5.27	−0.58	−0.78	0.7	1.12
2y	0.37	3.19	2.32	−0.86	−0.96	0.7	1.02
3y	0.63	3.24	4.98	1.95	1.72	0.6	1.02
4y	0.52	2.96	3.59	0.34	1.42	0.78	1.10
1x	0.74	3.32	3.6	−0.68	−1.69	0.88	1.32
2x	0.56	1.86	2.21	−0.05	1.36	0.96	1.27
3x	0.32	1.98	3..49	0.84	−0.98	0..45	1.15
4x	0.56	2.88	3.98	0.24	−0.69	0.72	1.06
5x	0.79	3.96	4.09	−0.19	−0.93	0.8	1.1
6x	0.66	2.03	4.02	0.38	−1.48	0.7	1.09
7x	0.86	2.37	1.48	0.83	−0.32	0.95	1.08
8x	0.82	1.36	5.67	0.87	−2.65	0.8	1.15

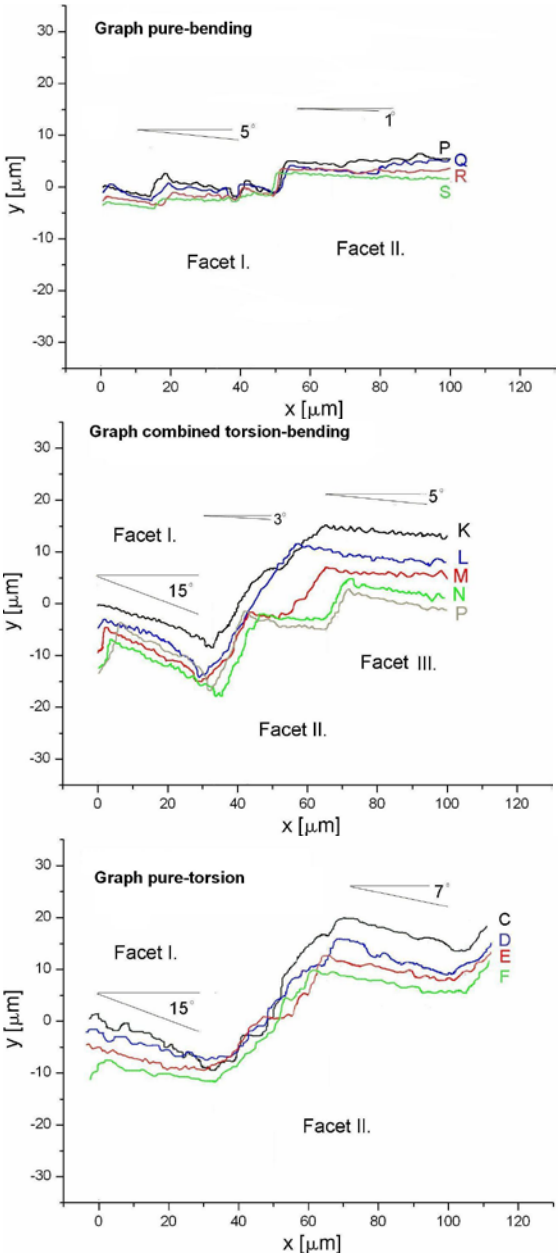

Figure 3. Topography of facets in Fig.2. Profiles for pure−bending (P: 1x−5x, Q: 2x−6x, R: 3x−7x,S: 4x−8x). Profiles for combined torsion−bending (K: 1x−9x, L: 2x−10x, M: x3−6x −11x, N: 4x−7x−12x, O: 5x−8x−13x). Profiles for pure−torsion (C: 1x−5x, D:2x−4x, E: 3x−7x , F:4x−8x).

Table 5 Profile roughness − bending−torsion. Z =0.73

Pr	R_V	R_a[μm]	R_q[μm]	R_{Sk}	R_{ku}	D	H
1y	0.45	3.06	3.36	0.12	−1.34	0.7	1.03
2y	0.27	2.70	3.79	0.19	−1.46	0.89	1.02
3y	0.42	4.26	4.77	−0.12	−1.59	0.7	1.02
4y	0.49	4.71	5.04	1.17	−0.37	0.67	1.02
5y	0.54	2.65	3.17	0.14	0.23	0.7	1.09
6y	0.56	4.74	5.03	0.13	−1.18	0.8	1.03
1x	0.49	3.77	4.53	−0.15	−1.62	0.8	1.03
2x	0.38	1.96	2.31	−0.14	−1.09	0.7	1.32
3x	0.20	0.22	0.28	−0.16	−1.01	0.68	1.07
4x	0.36	2.74	2.63	−0.12	−0.81	0.79	1.08
5x	0.41	1.02	1.17	0.14	−1.04	0.66	1.05
6x	0.77	4.53	4.56	−0.63	−1.18	0.7	1.03
7x	0.66	3.31	2.62	0.86	−1.35	0.8	1.12
8x	0.22	3.28	3.95	−0.17	−1.56	0.84	1.2
9x	0.37	3.56	3.75	1.12	−1.45	0.7	1.01
10x	0.34	3.37	3.05	0.38	−1.11	0.72	1.00
11x	0.29	3.57	3.75	−0.16	−1.19	0.8	1.13
12x	0.17	2.16	2.47	1.12	−0.54	0.7	1.03
13x	0.18	2.25	2.37	−0.17	−1.57	0.8	1.14

Table 5 Profile roughness – Pure torsion. $Z = 1$

Pr	R_V	R_a[μm]	R_q[μm]	R_{Sk}	R_{ku}	D	$_H$
1y	0.65	4.94	5.01	−0.13	−1.08	0.7	1.32
2y	0.53	5.38	5.41	0.16	−1.44	0.68	1.07
3y	0.41	3.23	4.03	0.14	−1.16	0.79	1.08
4y	0.76	4.73	5.04	−0.15	−1.47	0.66	1.05
5y	0.64	4.32	4.43	−0.13	−1.27	0.8	1.13
6y	0.54	4.32	4.45	−0.13	−1.31	0.7	1.03
7y	0.45	3.14	3.07	0.37	−1.35	0.8	1.14
8y	0.37	1.63	1.88	−0.30	−1.35	0.72	1.00
1x	0.37	1.70	2.74	1.13	1.24	0.7	1.03
2x	0.32	2.76	2.94	−0.15	−1.44	0.89	1.02
3x	0.45	3.14	4.07	0.37	−1.05	0.8	1.13
4x	0,36	3.85	3.99	−0.14	−1.05	0.7	1.32
5x	0.17	1.73	1.70	0.47	−1.42	0.7	1.03
6x	0.36	1.34	1.76	0.32	−1.06	0.89	1.13
7x	0.34	3.11	3.43	0.44	−1.30	0.9	1.03
8x	0.36	1.63	1.88	−0.13	−1.85	0.85	1.12

There is shown in Fig. 2 (combined bending−torsion $Z = 0.73$) fracture surface for combined bending−torsion loading. Along the Y−direction (starting from the profile K), the facet I changes its inclination to the macroscopic crack plane (a valley in between O and K), whereas facet III goes down steadily with an increasing slope, the small facet II dropped sharply with comparison to facet I – see Fig. 3 (combined bending−torsion). Along the X−direction, the facet I twists from the macroscopic (horizontal) plane by an angle of 15°. Twist angle of the facet III is about a third of that of the facet I and small facet II have twist angle 3°. Calculated values of roughness parameters are summarized in Table 5.

The roughness values R_a and R_q in the direction of the crack growth (profiles 1y−6y) are, in average, distinctly higher than those in the direction of the crack front (profiles 1x−13x). An increase of R_V, R_{Sk} and R_{ku} values can be observed in Y−direction (profiles 1y−6y) graduating from facet I to facet III. The skewness values approach the zero value typical for the normal distribution particularly on the facet I.

In Fig.2 c (pure−torsion) is shown fracture surface for pure−torsion loading. Along the Y−direction (from the profile C to profile F), the facet I down steadily with an constant slope – see Fig. 3 (pure−torsion). and facet II goes down steadily with an increasing slope– see Fig. 3. Along the X−direction,

the facet I twists from the macroscopic (horizontal) plane by an angle of 15°. Twist angle of the facet II is 7o. Calculated values of roughness parameters are summarized in Table 6. An decrease of R_V, R_{Sk} and R_{ku} values can be observed in X−direction (profiles 1x−8x) graduating from facet I to facet II.

VI. Discussion

In the case of pure−bending the crack propagates in the direction A under mixed mode I and II. In comparison to the combined bending torsion and pure−torsion is the fracture surface macroscopically In the case of combined torsion−bending loading, the crack front propagates in the direction A under the local mixed mode I+III along the facets I and III. The crack front on the facet II propagates in the direction A under mixed mode I and III, but effect of mode III decreased and possibly the effect of mode II on cracking slightly increased. Along the high step connecting facets (see Fig. 1), the front propagates in the direction B under the local mode I supported by the mode II. Such combination of mode I and II propagation in cases of prevailing torsion is necessary to prevent too high local deflections of the crack front from the horizontal plane.

In the case of pure−torsion, the crack front propagates in the direction A under the local mixed mode I/III along the facets I and II. Along the high step connecting facets (see Fig. 3), the front propagates in the direction B under the local mode I probably supported by the mode II. In comparison to low cycle fatigue (see [10]) the angle between y−axis and step connecting facets is higher (the angle 45^o for high cycle fatigue to 15^o for low cycle fatigue). Similar result can be found in [15−18].

VII. Conclusion

The presence of mode I in all propagation phases confirms a negligible importance of a single (pure) mode III crack growth mechanism in fatigue of metallic materials.

The roughness parameters R_L and R_q show that roughness of facets depended on the loading ratio and decreased with loading ratio *Z*. The roughness parameters in A−direction are clearly higher than the roughness parameters in B−direction.

Acknowledgment

The authors acknowledged the financial support: provided by the Czech Science Foundation in the frame of the Project No. SVV−2011−262901 and Specific research project of the Faculty of Science of University of Hradec Kralove.

References

[1] E.F. Underwood, K. Banerje. *Quantitative fractography* , In: Metals Handbook , 12th ed., Vol. 12, ASM International , 1992.

[2] D.F. Socie, G.B. Marquis, *Multiaxial Fatigue*, Warrendale, 2000.

[3] H. E. Exner, M. Fripan, M., Qauntitative assessment of three−dimensional roughness, anisotropy and angular distributions of fracture surfaces by stereometry, *Journal of Microscopy*, 78, 1985, pp. 138−161.

[4] J. Stampfl, R. Pippan, O. Kolednik, A New Powerful Tool for Surveying Cleavage Fracture Surfaces, *Fatigue Fract. Eng. Mater. Struct*., 1997, pp. 1541−1550.

[5] K.Slámečka, J.Pokluda, 3D Analysis of Fatigue Fracture Morphology Generated by Combined Bending−Torsion, In: Advenced Fracture Mechanics for Life and Safety Assesments, Stockholm, 2004.

[6] K.Slámečka, P. Ponížil, J.Pokluda, Quantitative fractography in bending−torsion fatigue, *Materials Science and Engineering* A 462 (2007), pp. 359–362

[7] T. Kobayashi**,** D.A. Shockey**,** Ch.G. Schmidt**,** R.W. Klopp**,** Assessment of fatigue load spectrum from fracture surface topography*". Int. J. Fatigue 19, 1997*, ***pp.*** 237−244.

[8] A. Vaziri, M. Nayeb−Hashemi, The effect of crack surface interaction on the Stress Intensity Factor in Mode III crack growth in round shafts, *Engineering Fracture Mechanics*, 2005, 72(4), pp. 617−629.

[9] Š. Major**,** P. Ponížil**.** K. Slámečka, J**.** Pokluda**,** 3D−Fractography in Bending− Torsion Fatigue. In Crack Paths**.** Parma: University of Parma**,** 2006**.** pp. 63−67.

[10] K. Slámečka, J**.** Pokluda, P**.** Ponížil, Š. Major, P. Šandera, On the topography of fracture surfaces in bending− torsion fatigue. *Engineering Fracture Mechanics*, 2007, Vol. 75, No. 1, pp. 760−767.

[11] Š.Major: Disertation: 2010, Brno University of Technology.

[12] W.P . Dong,. P.J. Stuliivan, K.J,Stullivan: Comprehersive study of paramtrs fir three−dmensuonal surface topograhgapy III:

[13] P. Ponížil , I. Saxl, Bernoulli Cluster Field: Voronoi Tessellation , *Applications of Mathematics.* 2002, vol. 47, issue 2, pp. 157−167

[14] E.S. Gadelmawla, M.M. Koura, T.M. Maksoud, I. M Elewa, H.H. Soliman, *J. Mat. Process. Technology* 123, 2002, pp. 133−145.

[15] A. S. Sayyad, Y. M. Ghugal, „*Flexure of Thick Beams using New Hyperbolic Shear Deformation Theory*". International Journal of Mechanics. Issue 3, Volume 5, 2011. pp. 113−122.

[16] B. Badri, M. Thomas, S. Sassi, „*A Shock Filter for Bearing Slipping Detection and Multiple Damage Diagnosis*". International Journal of Mechanics. Issue 4, Volume 5, 2011. pp. 318−326.

[17] Z. Boukria, A. Limam, „*Experimental Damage Analysis of Concrete Structures Using the Vibration Signature − Part II: Located Damage (Crack)*". International Journal of Mechanics. Issue 1, Volume 6, 2012. pp. 28−34.

[18] V. Lucia, G. Eugen, P. Vasile, „*Research on the Working Life at Steel Wire Ropes in Contact*". International Journal of Mechanics. Issue 1, Volume 6, 2012. pp. 140−147.